INFLUENCES FROM MGO-DOPED PHOSPHORS ON OPTICAL PROPERTIES OF WHITE LIGHT-EMITTING DIODES

Nguyen Thi Phuong Loan[1,*], *Ming-Jui Chen*[2]

[1]Faculty of Fundamental 2, Posts and Telecommunications Institute of Technology, Ho Chi Minh City, Vietnam.
[2]Department of Electrical Engineering, National Kaohsiung University of Science and Technology, Kaohsiung, Taiwan.

*Corresponding Author: Nguyen Thi Phuong Loan (Email: ntploan@ptithcm.edu.vn)
(Received: 16-November-2024; accepted: 05-June-2025; published: 30-June-2025)
http://dx.doi.org/10.55579/jaec.202592.480

Abstract. *MgO was produced utilizing Andrographis paniculata (A. paniculata), which forms cubic crystallites having a median dimension of 35 nm. SEM analysis shows the development of nano-bars (diameter - length: 46 nm - 185 nm). The illuminating spectra revealed oxygen deficiencies at 467 nm. This has high antimicrobial properties, having zones of restriction of 19 mm and 29 mm versus disease-causing agents from seafood and food. The compound has anti-udder cancer effect (IC50: 15.76 μg/mL for human mammary adenocarcinoma MCF-7) and is biocompatible.*

Keywords: *WLED; MgO; microfluidic technology; luminescence properties.*

1. Introduction

Metal oxide nanoparticles (NPs) are widely used in biomedical purposes such as medication and transmitting genes, tissue technology, diagnostics, and therapy. With these uses, assessing antimicrobial and anti-cancer properties may result in a low-cost cure and a simple drug having few adverse effects [1,2]. Illness from opportunistic aquatic infections including Vibrio cholerae, Streptococcus aureus, Aeromonas hydrophila, and Pseudomonas aeruginosa cause significant economic losses in fishery farming [3–5]. Furthermore, foodborne sickness creates significant health concerns in both underdeveloped and advanced regions. The Centers for Disease Control and Prevention (CDC, USA) have now identified E. coli, S. flexneri, S. aureus, and S. typhi as important foodborne pathogens [6–8].

The most often detected malignancies globally are mammary, pulmonary, and colorectal cancers. Mammary cancer remains the most common cancer in women globally. Numerous cancer treatments, including chemotherapy and radiotherapy, are ineffective and can harm normal tissues [9]. To restrict bacterial development and substitute current medications, investigators are looking for novel biocompatible pharmaceuticals having improved antimicrobial and cancer-fighting abilities [10].

MgO is a useful metal oxide with numerous applications, including catalysis, hazardous waste cleanup, refractory materials, materials for painting, and superconducting substances [11, 12]. MgO's non-toxicity makes it a popular choice for medical use [13, 14]. Microwave-supported green production is a sensitive and cost-effective alternative to physical and chemical processes. It is also environmentally benign. Umaralikhan et al. used plant extracts of P. guvajava and A. Vera to create MgO NPs with antimicrobial ability against S. aureus and E. coli [15]. Jeevanandam et al. produced MgO NPs using vegetal extracting using driven molecular nucleation [16]. Sugirtha et al. examined the curative effects of bioengineered MgO NPs on mankind cervical cancer cells having 31.2 $\mu g/mL$ IC50 factor [17]. YAG:Ce^{3+} (YGA:Ce), a common yellow phosphor applicable to apparatuses such as trackers, white illumination diodes, cathode beam pipes, etc., is employed in tandem with MgO to examine its optical attributes in experiments. This research aims to synthesize MgO nano-forms with A. Paniculata plant extraction as a stabilizer for antimicrobial and cancer-fighting uses against aquatic and foodborne pathogens, as well as to utilize the mankind udder cancer cell line MCF-7.

2. Experimental

For the extraction of the dark green dye, 10 g of A. paniculata leaves were cleaned in double distilled water and burned to 393 K over 30 minutes. The resulting substance was filtered twice to remove any remaining particles.

A. paniculata extracting substance was well combined with 0.5 M of $Mg(CH_3COO)_2{\cdot}4H_2O$. After 2 hours of stirring at 303 K, the mixture became transparent. The plant extraction was used for fuel, whereas the acetate in the forerunner acted like an oxidant. The obvious option was microwaved in a household oven during 20 minutes in convecting method. The grinding substance was calcined during 2 hours and thoroughly crushed to produce MgO nano-bars [18–20].

3. Results and discussion

It depicts the X-ray diffracting structure of MgO NRs from biotechnology. The cell factor is a = 0.4210 nm, having a face-centered cubic stage. The mean crystallite dimension (D = 35 nm) is determined by Debye Scherrer's equation [12]. The Williamson-Hall (W-H) plot indicates micro-strain. In the case of strain, the slope is non-zero. The computed figures for micro-strain (ϵ) and deviation density (δ) are 0.0018 and 7.9528 × 1014 $lines/m^2$, correspondingly [21]. The SEM picture reveals a bar-shaped form (dimension - lengthiness: 46 nm - 185 nm). EDS examination shows the Mg and O existence, with no maximum impurities. FTIR absorbing areas at 3443 and 1631 cm^{-1} correspond to OAH stretching and bending options, accordingly. The spectrum at 1383 cm^{-1} represents the bending vibration of the carbonyl group CO_3^{2-}, whereas the region at 511 cm^{-1}1 corresponds to the stretching Mg-O phase [13]. Illumination investigations indicate that emitted ranges at 449 and 467 nm are caused by oxygen problems.

Antimicrobial effectiveness was assessed against seafood (P. aeruginosa and V. cholerae) and food pathogens (E. coli, S. flexneri, S. aureus) at various doses. The ZOI showed up for both seafood and food pathogens. According to this work, MgO NRs demonstrated a larger regulation region against S. flexneri in comparison with the conventional antibiotic streptomycin. The findings have been contrasted to the ZOI of specific food bacterial variants for MgO NPs. The illuminating experiments show that emitted ranges at 449 and 467 nm are caused by oxygen vacancies, which increase the quantity of reactive oxygen species (ROS). Light-induced oxidative stress in bacterial cell walls generates ROS (OH^-, O_2^-, and H_2O_2) on the NPs outermost layer, resulting in cell death [22]. This is a widely acknowledged mechanism for antibacterial action. Mg^{2+} ions emitted from MgO NRs with not-uniform surfaces and rough edges may interact with the microbe's cell membrane. Negatively charged cell membranes attract Mg^{2+}. Mg^{2+} infiltrates the cell membrane and damages the S-H category, resulting in cell death.

The biocompatibility of MgO was assessed using normal cells, particularly RBCs. Green combined MgO NRs were tested for hemolytic effect on RBCs with doses of 20 and 40 $\mu g/mL$. MgO NRs exhibit negligible hemolytic action against RBCs at doses of 20 (1.17%) and 40 $\mu g/mL$ (2.86%), correspondingly. MgO NRs were

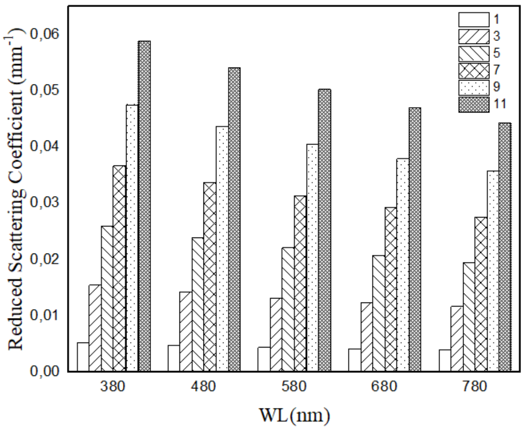

Fig. 1: Scattering coefficients with various wavelengths.

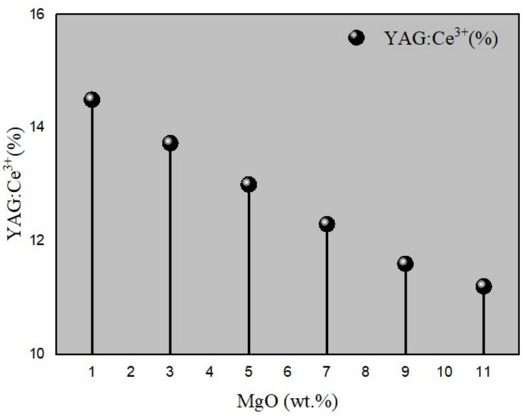

Fig. 2: YGA:Ce phosphor proportion values with different MgO proportions.

tested for their anti-breast cancer efficacy on cultured MCF-7 cells. The cells were exposed to a media with 5-100 $\mu g/mL$ dosage for 24 hours (p less than 0.05). The structural examination of the regulated and MgO NRs given to the MCF-7 mammary cancer cell line was carried out using an inverting microscope approach. Untreated cells using MgO NRs vary in comparison to those injected with NRs in terms of both count and morphology. Greater amounts of the examined cells result in a direct dose-response connection. MgO NRs at a minimal concentration of 15.76 $\mu g/mL$ can cause 50% cell death. Cancer cell death may happen through one mechanism: (i) ROS (.OH, $.O_2$ and H_2O_2) are important in eukaryotic cell death by MgO NRs. Hydroxyl radicals are strong oxidants that cause DNA harm, include sole and dual strand cracks, alterations, and oxidized nucleotides [17]. Fig. 1 illustrates

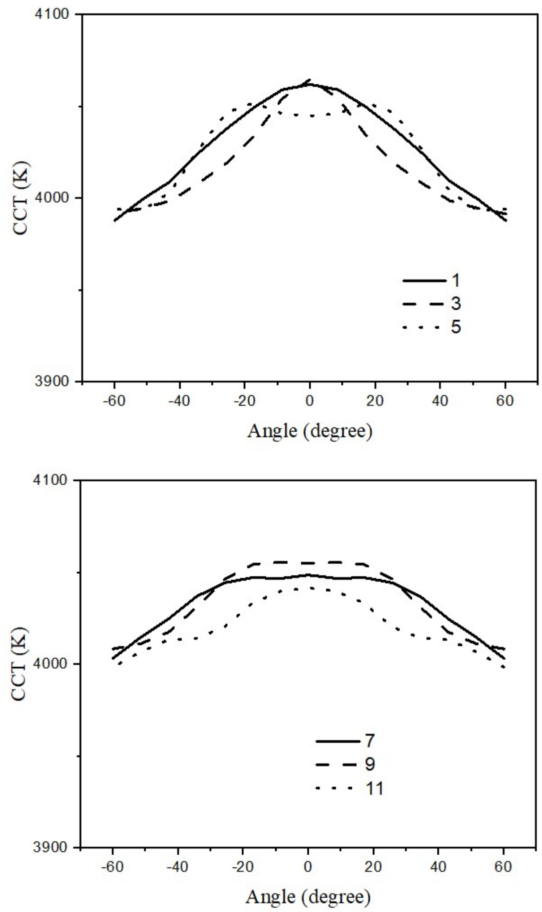

Fig. 3: CCT values with various MgO proportions.

the relationship between MgO dose and light dispersion. It increases MgO dosages by improving light transmission and wavelength conversion efficiency. When forward scattering and reabsorption are reduced and forward emission blue light dispersion rises, blue light brightness may rise. This is accomplished by increasing the MgO concentration and decreasing the yellow phosphorus concentration. Similarly, adjusting the color temperature (CCT) is limited [23–26]. CCT is concentration independent, as shown in Fig. 3 and Fig. 4; nevertheless, when the dosage of MgO increases, so does the dosage of YGA:Ce yellow phosphor, as illustrated in Fig. 2. Fig. 2 shows increasing MgO dosages (1-11 wt.%) and decreasing YGA:Ce phosphor ratios (from nearly 15% to just more than 11%). Fig. 3 shows how increased doping can reduce a phosphor's CCT variance. The maximum CCT values are seen at temperatures of over 4050 K and MgO concentrations of 9 wt.%. Fig. 4 shows that the D-CCT finally achieves its lowest value at 7 wt.% MgO, which is around 150 K lower than the maximum value at 11 wt.% MgO, which is around 200 K.

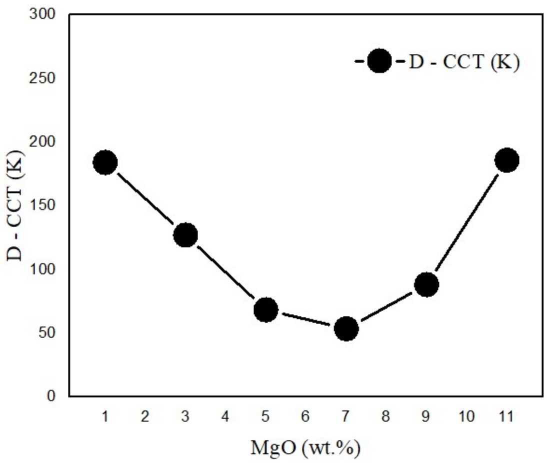

Fig. 4: YGA:Ce phosphor proportion values with different MgO proporColor difference values with different MgO proportions.

Fig. 5 demonstrates that adding MgO does not always boost the brightness of white light emissions. The highest results were obtained at a MgO concentration of 3 wt.%, whereas the poorest were produced at concentrations of 11 wt.%. Blue emission is diminished as a result of increased backscattering and reabsorption, and color distribution is irregular. Higher concentrations of MgO, for example, may cause the phosphor to change color from blue to yellow or orange-red when subjected to more backscattered blue light. Before the phosphor coating may expand, a specific amount of MgO is required. The emission spectrum would be limited by the multiple reflections the modified light would encounter from various objects. In other words, a high phosphor dose may increase the proportion of back-reflected converted light, increasing CCT while decreasing luminous intensity. Fig. 5 shows that 3 wt.% MgO increases brightness and color uniformity in a simulated WLED with a lumen output power of more than 130 lm. This WLED, simulated via LightTools, is identical to one used in an earlier study [27]. The concentration of MgO has a significant impact on the brightness and hue rendition of white LEDs, as seen in Fig. 6 and Fig. 7. Experiments with color rendition utilizing the color rendering indicator (CRI) and the color quality scale (CQS) revealed a consistent decrease as the MgO concentration increased to 11 wt.%. CRI and CQS reductions could be linked to the unpredictable nature of blue, green, and yellow-orange colors. High MgO concentrations generate irregular light emission, a bias toward the yellow-orange spectrum, and increased dispersion. As we examine the data, we will change the CRI and CQS of this phosphor while also taking into account other aspects such as particle size.

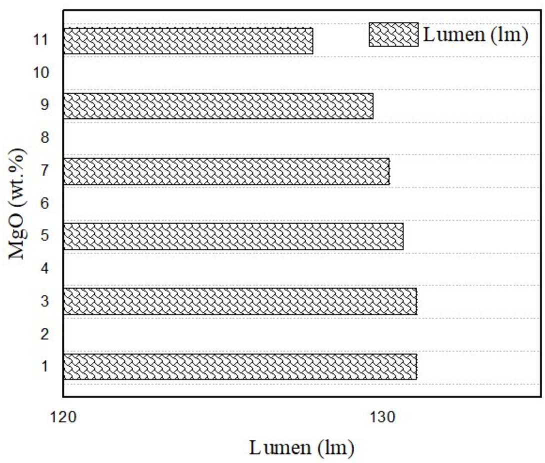

Fig. 5: Luminescence strength with various MgO proportions.

As our aforementioned results in Table 1 were collected from the study herein, they were compared to our earlier works that concern similar subjects involving LED apparatuses tested with other metal oxides, and luminescent phosphors to boost optical performance. For enhancing optical performance, the first work used for comparison utilizes luminescent phosphor $KBaYSi_2O_7$: Bi^{3+}, Eu^{3+} [28], while the second one features metal oxide ZnO [29]. As can be seen compared data, the scattering coefficient and YGA:Ce concentration outcomes under ef-

Tab. 1: CResult comparison of optical attributes influenced by particle sizes of metal oxides or luminescent phosphors.

Studies	Present study
Studies	Application of $KBaYSi_2O_7$:Bi^{3+},Eu^{3+} Phosphor for White Light-Emitting Diodes with Excellent Color Quality
Studies	ZnO-doped yellow phosphor compound for enhancing phosphor-conversion layer's performance in white LEDs
Scattering coefficient	Decreases with bigger particle sizes
Scattering coefficient	Initially shows little changes with smaller particle sizes, then polarized
Scattering coefficient	Initially shows little changes with smaller particle sizes, then polarized changes as particle size increases
YGA:Ce concentration	Decreases with bigger particle sizes
YGA:Ce concentration	Initially increases, decreases, then shows no fluctuations as particle size increases
YGA:Ce concentration	Initially increases, then decreases as particle size increases
CCT	Noticeable fluctuations with all particle sizes
CCT	Strong, polarizing fluctuations with most particle sizes
CCT	Initially shows huge fluctuations then smaller, more consistent fluctuations as particle size increases
Lumen	Decreases with bigger particle sizes
Lumen	Initially decreases, then increases, then minor fluctuations as particle size increases
Lumen	Initially increases, then decreases as particle size increases
CRI	Declines with bigger particle sizes
CRI	Initially declines, then increases, then shows huge fluctuations as particle size increases
CRI	Initially increases, then declines as particle size increases
CQS	Declines with bigger particle sizes
CQS	Initially declines, then increases, then shows minor fluctuations as particle size increases
CQS	Initially increases, then declines as particle size increases

fect of MgO are similar to that of the two compared studies. For CCT, MgO shows similar influences to ZnO, but its influences are far less pronounced with less chaotic fluctuations than $KBaYSi_2O_7$: Bi^{3+}, Eu^{3+}. This mechanism is also the same for lumen, CRI as well as CQS. As such, metal oxide MgO, similar to its counterpart ZnO, exerts more consistent influences on optical attributes than the aforementioned luminescent phosphor.

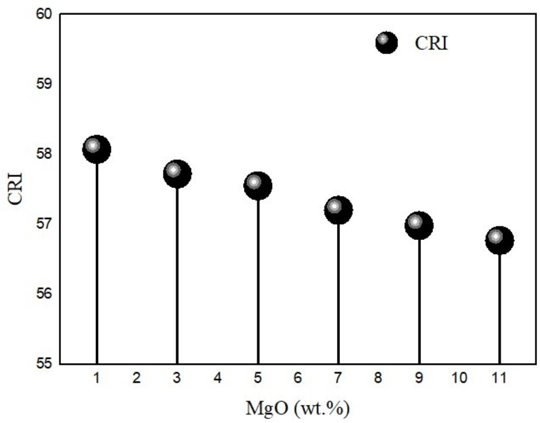

Fig. 6: CRI values with various MgO proportions.

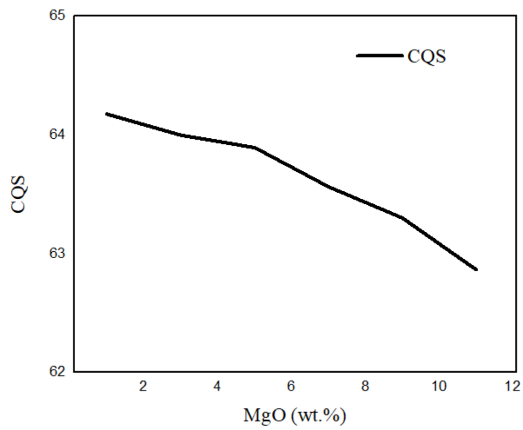

Fig. 7: CQS values with various MgO proportions.

4. Conclusion

MgO NRs from A. Paniculata leaf extracting were studied by XRD, FTIR, SEM with EDS, and FL. XRD shows a face-centered cubic form having a median crystallite dimension of 35 nm. SEM-based outer layer morphology supports the production of nanorods. MgO NRs exhibit substantial antimicrobial and cancer-fighting properties. The green production of MgO NRs is excellent for medical-biology purposes.

5. Acknowledgement

The author wishes to express their gratitude to the Posts and Telecommunications Institute of Technology, Vietnam, for financial support for this research.

References

[1] L.T. Chou et al. Compact multicolor two-photon fluorescence microscopy enabled by tailorable continuum generation from self-phase modulation and dispersive wave generation. *Opt. Express*, 30(22):40315, 2022.

[2] P. Fjodorow et al. Intracavity absorption spectroscopy of hcl isotopes, h_2o, ch_4, c_2h_4, and c_2h_6 in the 3.1–3.4 μ m spectral range using a cr:cdse laser. *Opt. Express*, 30(22):40347, 2022.

[3] C. Lv, C. Li, K. Xiao, and C. Gao. Interim connection space based on colorimetric values for spectral image compression and reproduction. *Opt. Express*, 30(22):40144, 2022.

[4] Y. Li, X. Shi, L. Yang, C. Pu, Q. Tan, Z. Yang, and H. Huang. Mc-gat: multi-layer collaborative generative adversarial transformer for cholangiocarcinoma classification from hyperspectral pathological images. *Biomed. Opt. Express*, 13(11):5794, 2022.

[5] K. Gaudfrin, J. Lopez, L. Gemini, M. Delaigue, C. Hönninger, R. Kling, and G. Duchateau. Fused silica ablation by double ultrashort laser pulses with dual wavelength and variable delays. *Opt. Express*, 30(22):40120, 2022.

[6] H. Zhang et al. Large scale transparency-adjustable mini-led display with recoverable color gamut by a highly transparent electrochromic shutter. *Opt. Express*, 30(22):39904, 2022.

[7] Q. Li, X. Xu, Y. Wu, D. Zou, Y. Yin, and T. Yu. Generation of single circularly polarized attosecond pulses from near-critical density plasma irradiated by a two-color co-rotating circularly polarized laser. *Opt. Express*, 30(22):40063, 2022.

[8] E. Förster, D. Stumpf, L. Werner, H. Hillmer, and R. Brunner. Hyperchromatic lens doublets with an extremely small equivalent abbe number employing diffractive elements and refractive materials with exceptional dispersion properties. *J. Opt. Soc. Am. A*, 39(11):1992, 2022.

[9] Y. Wei, M. Zhao, and Z. Yang. Silicon metasurface embedded fabry–perot cavity enables the high-quality transmission structural color. *Opt. Lett.*, 47(20),:5344, 2022.

[10] Q. Lu, Y. Ding, W. Wang, S. Liu, and M. Xu. Vis-nir superachromatic triplet design with five-color correction for a broadband interferometer. *Appl. Opt.*, 61(30),:8880, 2022.

[11] C.L. Bogh, A.J. Muhowski, M.D. Nelson, V.G.J. Rodgers, and J. P. Prineas. Measurement of recombination mechanisms in mid-infrared w-superlattices. *Opt. Mater. Express*, 12(11),:4261, 2022.

[12] Y. Zhang, Z. Wu, P. Lin, Y. Pan, Y. Wu, L. Zhang, and J. Huangfu. Hand gestures recognition in videos taken with a lensless camer. *Opt. Express*, 30(22):39520, 2022.

[13] L. Zhu, B. Yao, L. Deng, Y.Yang, G. Wang, C.Gu, and L. Xu. Evaluation of gamut enhancement in yellow regions and a choice of optimal wavelength for a rgby four-primary laser display system. *Opt. Express*, 30(21):38938, 2022.

[14] X. Bi, P. Wang, T. Wu, F. Zha, and P. Xu. Non-uniform illumination underwater image enhancement via events and frame fusion. *Appl. Opt.*, 61(29):8826, 2022.

[15] C. Fan, H. Zhao, Z. Zhao, J. Li, Y. Du, X. Yang, and L.Zhang. Single-shot quantitative phase imaging with phase modulation of a liquid crystal spatial light modulator (lc-slm) under white light illumination. *Opt. Lett.*, 47(20):5264, 2022.

[16] G. Li, Y. Liu, Q. Xu, H. Liang, and X. Wang. Deep learning enabled inverse design of nanocrystal-based optical diffusers for efficient white led lighting. *Appl. Opt.*, 61(29):8783, 2022.

[17] X. Wang, Y. Wu, D. Xu, B. Wen, Q. Lv, and X. Wu. Synthetic aperture rainbow refractometry. *Opt. Lett.*, 47(20):5272,, 2022.

[18] C. Lin, X. Yi, Z. Ji, D. Hou, and Y. Lin. Optimum display luminance under a wide range of ambient light for cockpit displays. *Opt. Express*, 30(21):38439, 2022.

[19] A.H. Nguyen, K L. Ly, C.Q. Li, and Z. Wang. Single-shot 3d shape acquisition using a learning-based structured-light technique. *Appl. Opt.*, 61(29):858, 2022.

[20] L. Chen, Z. Lee, G. Lin, Y. Wang, J. Wang, and W. Lai. On the measurement of remote sensing reflectance by a traditional above-water approach in small water bodies. *Appl. Opt.*, 61(29):8664, 2022.

[21] J. Chen, A. Wang, A. Pan, G. Zheng, C. Ma, and B. Yao. Rapid full-color fourier ptychographic microscopy via spatially filtered color transfer. *Photonics Res.*, 10(10):2410, 2022.

[22] C. Liu, Z. Zou, Y. Miao, and J. Qiu. Light field quality assessment based on aggregation learning of multiple visual features. *Opt. Express*, 30(21):38298, 2022.

[23] A. Kumari, P. Nayak, B. Patra, K. Venkatasubbaiah, and R. Das. Third-order nonlinear optical manifestations in an intramolecular proton transfer fluorophore due to tamm-plasmon based broadband optical absorbers. *J. Opt. Soc. Am. B*, 39(10):2857, 2022.

[24] S. Lin, P. Sun, H. Gao, and Z. Ju. Haze optical-model-based nighttime image dehazing by modifying attenuation and atmospheric light. *J. Opt. Soc. Am. A*, 39(10):1893, 2022.

[25] . Liang, G.Yang, S. Bai, C. Li, X. Li, Y. Wang, J. Huang, J. Ji, and Yongsheng Zhu. Efficient and tunable photoluminescence for terbium-doped rare-earth-based cs2naycl6 double perovskite. *Opt. Lett.*, 47(19):5176, 2022.

[26] X. Cao, Y. Lian, Z. Liu, H. Zhou, Bin Wang, W. Zhang, and B. Huang. Hyperspectral image super-resolution via a

multi-stage scheme without employing spatial degradation. *Opt. Lett.*, 47(19):5184, 2022.

[27] N.T.M. Hanh, N.T.P. Loan, and H.V. Ngoc. Enhancing light scattering effect of white leds with zno nanostructures. *Int. J. Electr. Comput. Eng. (IJECE)*, 11(5):3838, 2021.

[28] N.T.P. Loan, L.X. Thuy, N.L. Thai, H.Y. Lee, and P. H. Cong. Application of kbaysi2o7: Bi3+,eu3+ phosphor for white light-emitting diodes with excellent color quality. *Opt. Lett.*, 9(3):756, 2024.

[29] P H. Cong, L.X. Thuy, N.T.P. Loan, H.Y. Lee, and N.D.Q. Anh. Zno-doped yellow phosphor compound for enhancing phosphor-conversion layer's performance in white leds. *Optoelectron. Adv. Mat.*, 18(7-8):389, 2024.

About Authors

Nguyen Thi Phuong LOAN was born in Da Nang province. In 2006, She received her master degree from University of Natural Sciences. Her research interest is in optoelectronics. She has worked at the Faculty of Fundamental 2, Posts and Telecommunications Institute of Technology, Ho Chi Minh City, Vietnam.

Ming-Jui CHEN was born in Kaohsiung city, Taiwan. He has been working at the Department of Electrical Engineering, National Kaohsiung University of Science and Technology, Kaohsiung, Taiwan. His research interest is Quantum Physics and Materials Science.